

# Multi-Neutrino Entanglement and Correlations in Dense Neutrino Systems

Marc Illa<sup>1,\*</sup> and Martin J. Savage<sup>1,†</sup>

<sup>1</sup>*InQubator for Quantum Simulation (IQuS), Department of Physics, University of Washington, Seattle, WA 98195*

(Dated: June 1, 2023)

The time-evolution of multi-neutrino entanglement and correlations are studied in two-flavor collective neutrino oscillations, relevant for dense neutrino environments, building upon previous works. Specifically, simulations performed of systems with up to 12 neutrinos using Quantinuum’s H1-1 20 qubit trapped-ion quantum computer are used to compute  $n$ -tangles, and two- and three-body correlations, probing beyond mean-field descriptions.  $n$ -tangle re-scalings are found to converge for large system sizes, signaling the presence of genuine multi-neutrino entanglement.

In extreme astrophysical environments, such as those found in core-collapse supernovae, neutrino densities are sufficiently high to participate in the transport of energy and momentum, in local chemical compositions and in dynamics [1–5]. Coherent evolution of lepton flavors, that depends on self-interactions between neutrinos induced by weak interactions [6–10], plays an important role. First studies of the quantum correlations in coherent evolution of dense neutrino systems, beyond mean-field descriptions, are providing important insights into such dynamics [11–28]. So far, they have focused on bipartite entanglement witnesses, such as entanglement entropy, negativity and concurrence [15–19, 21–26]. In this work, we explore multi-neutrino entanglement in such systems by computing  $n$ -tangles [29],  $\tau_n$ , between  $n$  neutrinos induced by time evolution. The total  $n$ -tangles at late times are found to scale for large system sizes. Our work utilized classical simulations, and quantum simulations using the Quantinuum 20-qubit trapped-ion quantum computer H1-1 and noisy emulator H1-1E [30].

The leading-order low-energy effective Hamiltonian describing collective, coherent neutrino flavor oscillations is composed of three terms. One term is responsible for vacuum oscillations, originating from the neutrino mass matrix [31–34]. A second is from the weak interactions between neutrinos and matter, mainly between  $\nu_e$  and  $e^-$ , through charged-current processes, and is responsible for the Mikheev-Smirnov-Wolfenstein effect [35, 36]. In what follows, we neglect the contributions from this term. A third term, from the neutral-current weak interactions, is responsible for coherent forward scattering of neutrinos, which becomes significant at sufficiently high neutrino densities [7–10].

Due to the small value of  $\theta_{13}$  [37], three-flavor neutrino systems can be approximated by two-flavor systems involving the electron neutrino  $\nu_e$  and a heavy neutrino  $\nu_x$ , considered to be a combination of  $\nu_\mu$  and  $\nu_\tau$  [38]. The effective Hamiltonian for  $N$  neutrinos can be written in terms of spin operators acting in flavor space [14],

$$H = H^\nu + H^{\nu\nu} = \sum_i \mathbf{b} \cdot \boldsymbol{\sigma}^{(i)} + \frac{1}{N} \sum_{i < j} J_{ij} \boldsymbol{\sigma}^{(i)} \cdot \boldsymbol{\sigma}^{(j)}, \quad (1)$$

where  $\boldsymbol{\sigma}^{(i)} = (\sigma_x^{(i)}, \sigma_y^{(i)}, \sigma_z^{(i)})$  are the Pauli matrices acting

on the  $i^{\text{th}}$  neutrino flavor-doublet,  $(|\nu_e\rangle, |\nu_x\rangle)^T$ . The 3-vector  $\mathbf{b}$  encodes the vacuum oscillations,

$$\mathbf{b} = \frac{\Delta m^2}{4E} (\sin(2\theta_v), 0, -\cos(2\theta_v)), \quad (2)$$

with  $\Delta m^2$  being the difference between neutrino squared-masses,  $E$  the neutrino energy, and  $\theta_v$  the vacuum-mixing angle. The two-body couplings  $J_{ij}$ , uniquely defined at leading order by the Standard Model, are,

$$J_{ij} = \sqrt{2} G_F \rho_\nu (1 - \cos \theta_{ij}), \quad (3)$$

where  $G_F$  is Fermi’s constant,  $\rho_\nu$  the number-density of neutrinos, and  $\theta_{ij}$  the angle of the momenta between the  $i^{\text{th}}$  and  $j^{\text{th}}$  neutrino. Following previous works, e.g., Refs. [18, 28], we introduce  $\mu \equiv \sqrt{2} G_F \rho_\nu$ , and, for demonstrative purposes, set  $\mu/N = \Delta m^2/4E$  (assuming a monochromatic beam), so that the one- and two-body terms have comparable strengths [18]. Following the inspiring work of Hall *et al.* [18], a one-parameter set is used to demonstrate relevant physics, with a vacuum-mixing angle of  $\theta_v = 0.195$ , a distribution of momenta with  $\theta_{ij} = \arccos(0.9) \times |i - j|/(N - 1)$  (cone-shaped), and an initial state that is a product state of  $N/2$   $|\nu_e\rangle$  and  $N/2$   $|\nu_x\rangle$ , i.e.,  $|\Psi_0\rangle = |\nu_e\rangle^{\otimes N/2} \otimes |\nu_x\rangle^{\otimes N/2}$ .

While a number of previous calculations of neutrino systems using quantum devices have been focused on the coherent time evolution of the flavor content [18, 20, 25, 28], and the entanglement of one or two neutrinos [18, 25], here we examine correlations between different neutrinos and multi-body entanglement, quantities that can further probe mean-field descriptions of these systems. Specifically, we look at the two-body correlations, as considered previously, e.g., Ref. [26],

$$\mathcal{C}_{ij}^{(2\nu)}(t) = \langle \sigma_z^{(i)} \sigma_z^{(j)} \rangle - \langle \sigma_z^{(i)} \rangle \langle \sigma_z^{(j)} \rangle, \quad i \neq j, \quad (4)$$

with  $\langle \cdot \rangle = \langle \Psi_t | \cdot | \Psi_t \rangle$ , and three-body correlations,

$$\begin{aligned} \mathcal{C}_{ijk}^{(3\nu)}(t) &= \langle \sigma_z^{(i)} \sigma_z^{(j)} \sigma_z^{(k)} \rangle - \langle \sigma_z^{(i)} \rangle \langle \sigma_z^{(j)} \sigma_z^{(k)} \rangle \\ &\quad - \langle \sigma_z^{(j)} \rangle \langle \sigma_z^{(i)} \sigma_z^{(k)} \rangle - \langle \sigma_z^{(k)} \rangle \langle \sigma_z^{(i)} \sigma_z^{(j)} \rangle \\ &\quad + 2 \langle \sigma_z^{(i)} \rangle \langle \sigma_z^{(j)} \rangle \langle \sigma_z^{(k)} \rangle, \quad i \neq j \neq k. \end{aligned} \quad (5)$$

Ultimately, studies of entanglement will help quantify the limitations of classical techniques in providing reliable and accurate results, and can also guide tensor-networks approaches [17, 19, 24]. Entanglement in neutrino systems has been previously computed via full-state tomography [18, 25], which, however, is expected to become inefficient for larger systems due to the required number of measurements. Alternative methods including classical shadows [39], which are expected to require fewer measurements, are currently being pursued.

As a way to gain further insight into the entanglement structure of dense, coherent neutrino systems, we focus on the  $n$ -tangle  $\tau_n$ , defined as  $|\langle \Psi | \sigma_y^{\otimes n} | \Psi^* \rangle|^2$ , where  $|\Psi^*\rangle$  is the complex conjugate of  $|\Psi\rangle$ . This quantity is a measure of the  $n$ -body entanglement [29]. For two-qubit (neutrino) systems,  $\tau_2$  is the concurrence squared [40, 41],  $C_{12}^2$ . For three-qubit systems,  $\tau_3$  is the residual entanglement [42],  $C_{1(23)}^2 - C_{12}^2 - C_{13}^2$ , with  $C_{1(23)} = \sqrt{2 - 2\text{Tr}\rho_1^2}$ , with  $\rho_1$  the reduced density matrix of the first qubit. However, for  $n \geq 4$ ,  $\tau_n$  is not uniquely the residual entanglement, and it is smaller than or equal to the concurrence  $C_{1(2\dots n)}$  [43]. An interesting property of  $\tau_n$  is that, for the  $N$ -qubit GHZ state [44, 45],  $\tau_N = 1$ , while for the  $N$ -qubit W state [46],  $\tau_N = 0$ . Thus, while it can help distinguish between different types of entanglement, by itself it is not a measure of  $N$ -body entanglement [29].<sup>1</sup>

*Implementation on a Quantum Computer* — Previous works have performed quantum simulations of these systems using IBM’s superconducting-qubit quantum computers [18, 20], D-Wave’s superconducting-qubit annealing devices [25] and Quantinuum’s Trapped-ion quantum computers [28]. We implement the time evolution of an initial state  $\Psi_0$  under the Hamiltonian given in Eq. (1) using Quantinuum’s H1-1 20 qubit trapped-ion quantum computer, that is based on using the two hyperfine clock states in the  $^2S_{1/2}$  ground state of  $^{172}\text{Yb}^+$  ions as qubits [30]. For purposes of comparison, we also provide results obtained using its emulator, H1-1E.<sup>2</sup> The evolution operator,  $\exp(-itH)$ , is Trotterized, and each contribution is mapped to a quantum circuit composed of gates that are native to H1-1. As noted in Ref. [28], the one-body and two-body parts of the Hamiltonian commute,  $[H^\nu, H^{\nu\nu}] = 0$ , so they can be Trotterized without introducing a higher-order systematic error. For  $H^\nu$ ,

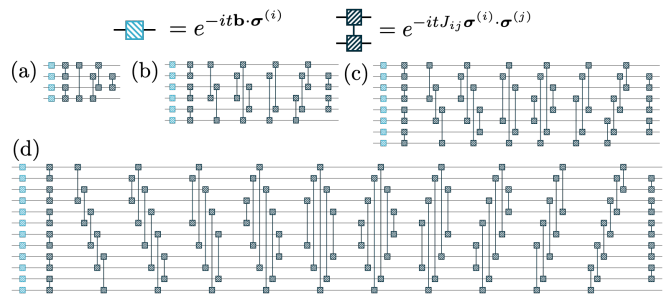


FIG. 1. Circuits for a single Trotter step for (a)  $N = 4$ , (b)  $N = 6$ , (c)  $N = 8$ , and (d)  $N = 12$  neutrinos, where the two-neutrino gates are clustered into groups that can be applied in parallel, showing the linear scaling with  $N$  of the circuit depth.

since each term acts on a different neutrino,

$$e^{-itH^\nu} = \bigotimes_i e^{-it\mathbf{b}\cdot\sigma^{(i)}}. \quad (6)$$

This term is implemented with the following Euler decomposition for  $SU(2)$  matrices [50],

$$e^{-it\mathbf{b}\cdot\sigma^{(i)}} = \boxed{R_z(\alpha_1)} \boxed{R_y(\alpha_2)} \boxed{R_z(\alpha_3)}, \quad (7)$$

where the angles  $\alpha_i$  are fixed numerically.

For  $H^{\nu\nu}$ , the known decomposition of  $SU(4)$  matrices with 3 CNOT gates [51] is used,

$$e^{-itJ_{ij}\sigma^{(i)}\cdot\sigma^{(j)}} = \begin{array}{c} \text{---} \oplus \boxed{R_z(\beta - \frac{\pi}{2})} \text{---} \\ \boxed{R_z(\frac{\pi}{2})} \text{---} \bullet \text{---} \oplus \boxed{R_z(\beta - \frac{\pi}{2})} \text{---} \\ \text{---} \oplus \boxed{R_z(\frac{\pi}{2})} \text{---} \bullet \text{---} \oplus \boxed{R_z(\beta - \frac{\pi}{2})} \text{---} \\ \text{---} \oplus \boxed{R_z(\beta - \frac{\pi}{2})} \text{---} \end{array}, \quad (8)$$

with  $\beta = 2tJ_{ij}$ , which has a slight advantage over [52, 53] (requiring 5 single-qubits gates instead of 8). While not directly relevant to the present set of simulation, it is interesting to consider the T-gate resource requirements for such simulation. Standard methods<sup>3</sup> suggest a T-gate count of  $N(187N - 101)/2$  for  $\epsilon = 10^{-4}$ , for  $N$  neutrinos per Trotter step. While the circuits in Eqs. (7) and (8) are not written in terms of the native gates used in H1-1 (these can be found in Ref. [28]), the package `pytket` [58] includes a function that performs this translation, along with optimizations. Implementation of this two-neutrino term is more delicate. Since the sum over different pairs of neutrinos is split in the implementation of the time-evolution operator, the non-commutativity of terms introduces systematic Trotter errors. While it is possible

<sup>1</sup> There are other ways to ascertain the nature of entanglement in these systems. For example, a more complete set of two-point correlation functions could be used to determine the Quantum Fisher information,  $F = \sum_{\alpha,\beta} \sum_{i,j} n_\alpha^i C_{\alpha,\beta}^{i,j} n_\beta^j$ , with  $n_\alpha^i$  being unit vectors and  $C_{\alpha,\beta}^{i,j} = \langle \sigma_\alpha^{(i)} \sigma_\beta^{(j)} \rangle - \langle \sigma_\alpha^{(i)} \rangle \langle \sigma_\beta^{(j)} \rangle$ , which can be used to learn about the nature of entanglement [47, 48].

<sup>2</sup> Ref. [49] showed that H1-1E could well reproduce the behavior of H1-1.

<sup>3</sup> Following Ref. [54], and assuming no additional ancilla qubits are used, for general single-qubit rotations  $U_1$ , Refs. [55, 56] give the following estimates of the number of T-gates,  $T_{U_1}(\epsilon) = 2.95 \log_2(1/\epsilon) + 3.75$ . For  $R_z$ , Ref. [57] gives  $T_{R_z}(\epsilon) = 3.21 \log_2(1/\epsilon) - 6.93$ .

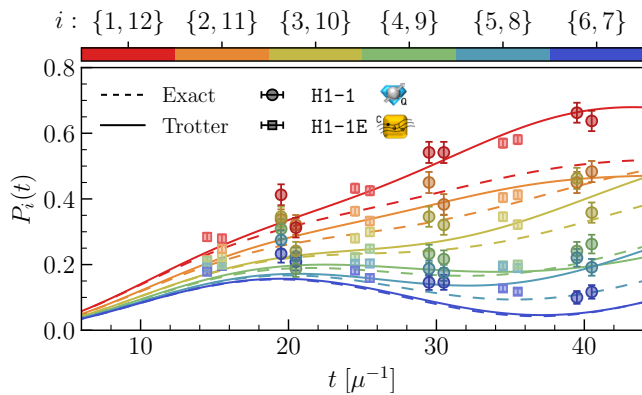


FIG. 2. Flavor inversion probabilities for  $N = 12$  neutrinos. The lines show the single-step Trotter (continuous) and exact (dashed) simulations, and the points show the results from H1-1 (dark circles, using 240 shots) and H1-1E (light squares, using 1200 shots).

to find a combination that minimizes this error, as in Ref. [28] for the case of 4 neutrinos, this is not feasible for larger systems. As shown in Ref. [18], it is possible to build a circuit that performs the Trotterized version of  $\exp(-itH^{\nu\nu})$  with  $N$  layers of the operator in Eq. (8) (if multiple gates can be applied in parallel across the device). Figure 1 shows the circuits used for different number of neutrinos. A nice property of these circuits is that they retain the symmetry present in the Hamiltonian given in Eq. (1), between the exchange of the  $i^{\text{th}}$  and  $(N - i + 1)^{\text{th}}$  neutrino, for the current choice of  $J_{ij}$ . While first order Trotter evolution has been used, higher orders with their improved convergence have been explored in Ref. [28]. They found that the Trotter errors from first and second order evolution from the prepared initial state are significantly smaller than naive theoretical bounds. Alternative methods for time evolution, such as Variational Fast Forwarding [59], should also be examined.

*Two- and Three-Neutrino Correlations* — A term that appears in the computation of correlation functions is the expectation value of  $\sigma_z$ . For this reason, it is interesting to first compute the inversion probability for a single neutrino, defined as

$$P_i(t) = \frac{1}{2}(1 \mp \langle \sigma_z^{(i)} \rangle), \quad (9)$$

where the  $\mp$  sign depends on the initial state of the  $i^{\text{th}}$  neutrino ( $-$  for  $\nu_e$  and  $+$  for  $\nu_x$ ). Due to the symmetry of the Hamiltonian (and its Trotterized version), the inversion probabilities for the  $i^{\text{th}}$  and  $(N - i + 1)^{\text{th}}$  neutrino are the same. The results for  $N = 12$  are shown in Fig. 2, where the two icons in the legend indicate whether a quantum device (blue) or emulator (yellow) was used to obtain the results [60], and the  $N = 8$  are in the Supplemental Material (SM). The uncertainties in the results

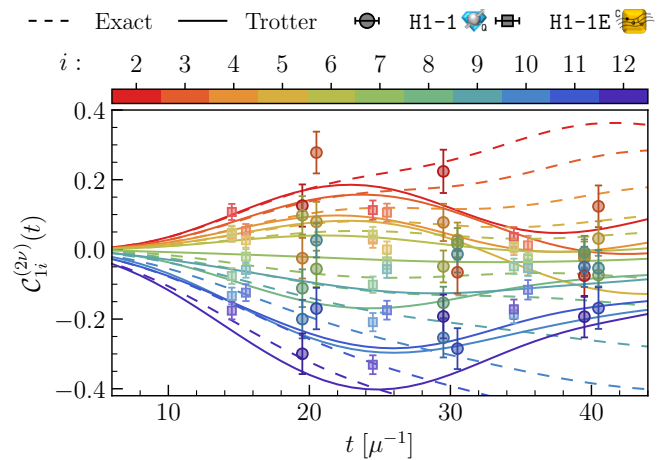


FIG. 3. Two-body correlation for  $N = 12$  neutrinos. The lines show the single-step Trotter (continuous) or exact (dashed) simulation, and the points show the results from H1-1 (dark circles, using 240 shots) and H1-1E (light squares, using 1200 shots).

are computed via bootstrap resampling. For the  $N = 8$  case, agreement is found with the results presented in Ref. [28]. For  $N = 12$ , both results from H1-1 and H1-1E are showing somewhat larger deviations from expectations, but the device has remained coherent.<sup>4</sup>

As a selection of two- and three-body correlations, we focus on

$$\begin{aligned} & \mathcal{C}_{1i}^{(2\nu)}, \text{ with } 1 < i \leq N, \quad \mathcal{C}_{1iN}^{(3\nu)}, \text{ with } 1 < i < N, \\ & \mathcal{C}_{i,i+1}^{(2\nu)}, \text{ with } 1 \leq i < N, \quad \mathcal{C}_{i-1,i,i+1}^{(3\nu)}, \text{ with } 1 < i < N. \end{aligned}$$

A representative set of correlation functions for  $N = 12$  neutrinos is shown in Fig. 3, and a more complete set can be found in the SM. For the two-body correlations, results from H1-1 and H1-1E follow the expected values, although somewhat limited by statistics. This gets more prominent when looking at the three-body correlations, where with the current uncertainties most of the points are consistent with zero. As seen by comparing the results from H1-1 and H1-1E, increasing the accumulated statistics by factor of 5 makes a substantial difference, but it remains insufficient. Increasing further the number of shots would help resolve those small values, which would be reasonable with, for instance, IBM's quantum computers (where usually one works with  $\gtrsim 10^4$  shots). With the possibility of performing more shots, error mitigation techniques, such as randomized compiling [61] and decoherence renormalization [62–64], become viable. While these correlations differ from zero, with a hierarchy  $\mathcal{C}^{(2\nu)} > \mathcal{C}^{(3\nu)}$ , an interesting trend is that  $\mathcal{C}_{1i}^{(2\nu)}$  plateaus

<sup>4</sup> The associated SM gives the numerical values of the results shown in Fig. 2, and those shown in subsequent figures.

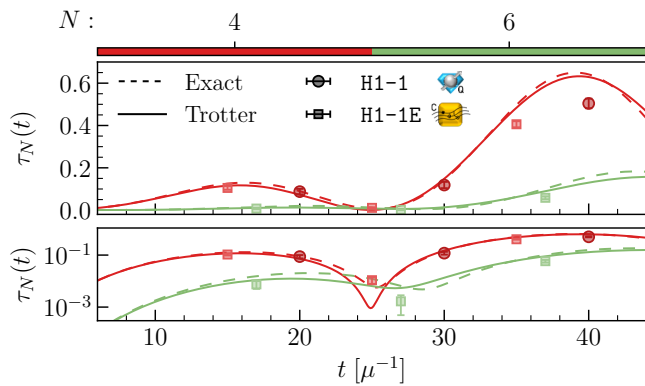


FIG. 4.  $N$ -tangle  $\tau_N$  for  $N = \{4, 6\}$  neutrinos on a linear (top) and log (bottom) scale. The lines show the Trotter (continuous) or exact (dashed) simulation, and the points show the results from H1-1 (dark circles, using 480 shots) and H1-1E (light squares, using 1200 shots).

at late times, with  $C_{12}^{(2\nu)}$  reaching a value  $\sim 0.5$ , down to  $\sim -0.5$  for  $C_{1N}^{(2\nu)}$ . Other limiting patterns are not found for other computed quantities.

A potential improvement to the current results has been explored, in which a post-selection of the counts that satisfy the symmetries of the Hamiltonian. This technique has been used with great success when studying quantum field theories, e.g., see Refs. [49, 64–66]. However, specific to this system in the flavor basis,  $\mathbf{b} \cdot \mathbf{J}$  is the conserved quantity (and not  $J_z$ ), which makes post-selection not feasible in our studies.<sup>5</sup>

*Multi-Neutrino Entanglement* — The  $N$ -tangle,  $\tau_N$ , is an interesting measure of multi-neutrino entanglement in these systems which is straightforward to compute via,

$$\tau_N(t) = |\langle \Psi_t | \sigma_y^{\otimes N} | \Psi_t^* \rangle|^2 = |\langle \Psi_0 | e^{itH} \sigma_y^{\otimes N} e^{-itH} | \Psi_0 \rangle|^2, \quad (10)$$

(without the need to use the SWAP test [67–69] to compute the overlap). We have performed such calculations for the system of  $N = 4$  neutrinos using H1-1 and H1-1E, as shown in the top panel of Fig. 4, where two Trotter steps have been used in applying  $e^{itH}$ . The  $N = 6$  system has also been studied, but only using H1-1E (and with a single Trotter step). For the time-range displayed,  $\tau_N$  is seen to decrease rapidly with system size.

To further explore the dependence of multi-neutrino entanglement with system size, it is interesting to look at  $\tau_n$ , with  $n < N$ . For this quantity, a re-scaling of the sum of the  $\tau_n$ s is found to be helpful,

$$\tilde{\tau}_{n,N} = \frac{1}{N^{n-2}} \sum_i \tau_n^{(i)}, \quad (11)$$

<sup>5</sup> Calculations could be performed in the mass basis, but the selected initial state would then be a sum of product states, which would complicate the calculation of the  $n$ -tangle.

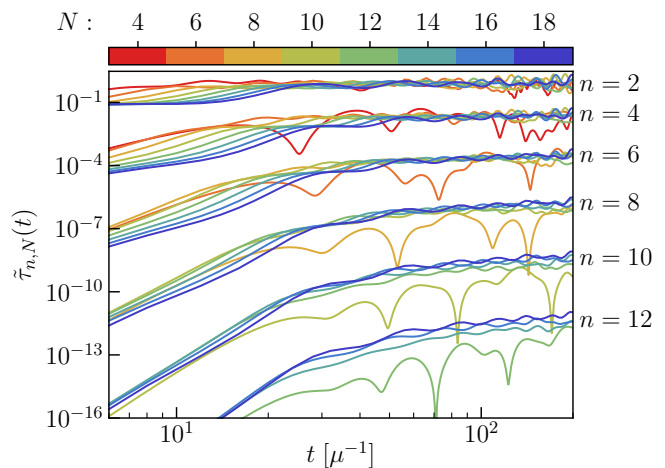


FIG. 5. The re-scaled  $n$ -tangle,  $\tilde{\tau}_{n,N}$ , defined in Eq. (11), for  $n = \{2, \dots, 12\}$  and  $N = \{4, \dots, 18\}$  neutrinos.

where the index  $i$  in  $\tau_n^{(i)}$  identifies one of the possible  $\binom{N}{n}$  permutations of  $\sigma_y^{\otimes n}$ .<sup>6</sup> Figure 5 shows the re-scaled  $\tilde{\tau}_{n,N}$  for different values of  $N$  and  $n$ . These quantities are seen to exhibit convergence to a fixed curve with increasing  $N$ , starting for relatively small system sizes. The time required to reach the plateau region increases with  $n$ , consistent with the notion that more time is required to entangle  $n$  neutrinos than  $n - 1$ . Moreover, upon further investigation, these plateaus are found to be robust against variations of the two-body coupling strength (increasing or decreasing the angle of the cone) and vacuum-mixing angle (more or less oscillatory behavior), the only observed difference is in the relaxation time (shorter times for wider cones because the interaction strength  $J_{ij}$  is stronger).

While this scaling is somewhat puzzling, it can be compared to other entangled multiqubit systems, for which analytic results are available. For example, the GHZ state has  $\tau_{n=N} = 1$  and  $\tau_{n < N} = 0$ , while the W state has  $\tau_n = 0 \forall n$  except for  $\tau_{n=2} = 2(N-1)/N$  (with  $\tau_n = \sum_i \tau_n^{(i)}$  for  $n < N$ ). A system that has similar scaling is the product of  $N/2$  Bell pairs, with  $\tau_n = \binom{N/2}{N/2-n/2} \sim N^{n/2}$ . Comparing this with the scaling from Eq. (11), the  $n$ -tangle grows faster for the neutrino state than the Bell-pairs-state with system size (except for  $\tau_2$  and  $\tau_4$ ), as depicted in Fig. 6. This implies that there is multi-neutrino entanglement, beyond the two-neutrino entanglement found in the  $(N/2)$ -product Bell-pairs-state.

The present analysis concerns the coherent flavor oscillations of a mono-energetic neutrino gas starting in a mixed-flavor pure state. To gain an understanding of such dynamics in a mixed state, we have also examined

<sup>6</sup> e.g., for  $N = 4$  and  $n = 2$ , these are  $\sigma_y \otimes \sigma_y \otimes I \otimes I$ ,  $\sigma_y \otimes I \otimes \sigma_y \otimes I$ ,...

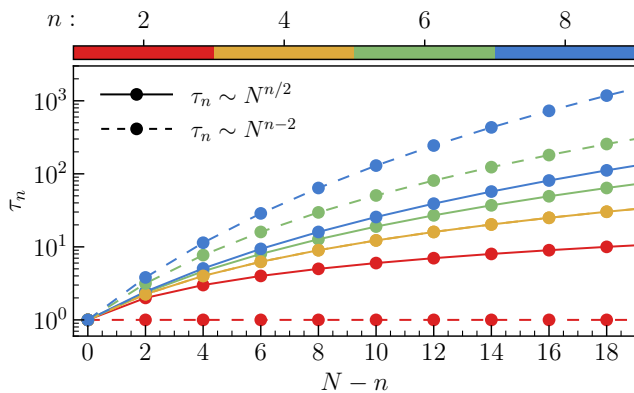


FIG. 6. Comparison of two scalings of the  $n$ -tangles,  $N^{n/2}$  (continuous line) as found for systems of Bell pairs, and  $N^{n-2}$  (dashed line) as we have identified from the time evolution, for different values of  $n$  and system sizes  $N$ , normalized to  $\tau_{n=N} = 1$ .

the impact of different initial states for the evolution, and find that the values of  $n$ -tangle depend upon the initial state in non-trivial ways. A mono-flavor initial state gives vanishing  $n$ -tangle, while an initial state with a single distinct flavor has non-zero 2-tangle, resembling a W-state (the oscillations are too large to discriminate between the different  $N$ -scalings, consistent with  $2(N-1)/N$  or  $N^{n-2}$ ). Gases of different energy neutrinos can be described within this framework through different values of  $\mathbf{b}$  in Eq. (2).

*Summary and Conclusions* — The time evolution of multi-neutrino quantum correlations and entanglement in dense neutrino systems is studied for systems of  $N = 4, 6, 8$  and 12 neutrinos using Quantinuum’s H1-1 20 qubit trapped ion quantum computer and its associated noisy emulator H1-1E. The central reason for including and developing methods for implementation on quantum computers is that determining the entanglement of the larger systems that will be required as input into realistic astrophysical simulations will need quantum simulations of such systems with larger numbers of neutrinos (than in this work). We have chosen to study the  $n$ -tangle in order to provide insight into the multi-particle entanglement structure of the systems. Compared to other entanglement witnesses, the  $n$ -tangle is straightforward to compute using a quantum computer (at least for a single product state, as considered here), since it does not require state tomography. The behavior of re-scaled sums over  $n$ -tangles are found to converge to universal curves with increasing system sizes, that depend upon the parameters of the Hamiltonian, with late-time plateaus. Further, the magnitudes of the  $n$ -tangles are found to increasingly exceed that of systems comprised of neutrino Bell-pairs, indicating the presence of genuine multi-neutrino entanglement in collective coherent neutrino flavor oscillations in dense systems.

*Acknowledgements* — We would like to thank Valentina Amitrano, Ramya Bhaskar, Joe Carlson, Anthony Ciavarella, Roland Farrell, Francesco Pederiva, Alessandro Roggero and Francesco Turro, along with the QSC Thrust-2 team, for insightful discussions. This work was supported in part by the U.S. Department of Energy, Office of Science, Office of Nuclear Physics, InQubator for Quantum Simulation (IQUS) (<https://iqus.uw.edu>) under Award Number DOE (NP) Award DE-SC0020970 (Savage), and the Quantum Science Center (QSC) (<https://qscience.org>), a National Quantum Information Science Research Center of the U.S. Department of Energy (DOE) (Illa). This work is also supported, in part, through the Department of Physics (<https://phys.washington.edu>) and the College of Arts and Sciences (<https://www.artsci.washington.edu>) at the University of Washington. This research used resources of the Oak Ridge Leadership Computing Facility, which is a DOE Office of Science User Facility supported under Contract DE-AC05-00OR22725. We have made extensive use of Wolfram Mathematica [70], Python [71, 72], Jupyter Notebooks [73] in the Conda environment [74], Julia [75–77] and the quantum programming environments: IBM’s qiskit [78] and CQC’s pytket [58].

\* [marcilla@uw.edu](mailto:marcilla@uw.edu)

† [mjs5@uw.edu](mailto:mjs5@uw.edu)

- [1] H. Duan and J. P. Kneller, Neutrino flavour transformation in supernovae, *J. Phys. G* **36**, 113201 (2009), [arXiv:0904.0974 \[astro-ph.HE\]](https://arxiv.org/abs/0904.0974).
- [2] H. Duan, G. M. Fuller, and Y.-Z. Qian, Collective Neutrino Oscillations, *Ann. Rev. Nucl. Part. Sci.* **60**, 569 (2010), [arXiv:1001.2799 \[hep-ph\]](https://arxiv.org/abs/1001.2799).
- [3] S. Chakraborty, R. Hansen, I. Izaguirre, and G. Raffelt, Collective neutrino flavor conversion: Recent developments, *Nucl. Phys. B* **908**, 366 (2016), [arXiv:1602.02766 \[hep-ph\]](https://arxiv.org/abs/1602.02766).
- [4] I. Tamborra and S. Shalgar, New Developments in Flavor Evolution of a Dense Neutrino Gas, *Ann. Rev. Nucl. Part. Sci.* **71**, 165 (2021), [arXiv:2011.01948 \[astro-ph.HE\]](https://arxiv.org/abs/2011.01948).
- [5] F. Capozzi and N. Saviano, Neutrino Flavor Conversions in High-Density Astrophysical and Cosmological Environments, *Universe* **8**, 94 (2022), [arXiv:2202.02494 \[hep-ph\]](https://arxiv.org/abs/2202.02494).
- [6] G. M. Fuller, R. W. Mayle, J. R. Wilson, and D. N. Schramm, Resonant Neutrino Oscillations and Stellar Collapse, *Astrophys. J.* **322**, 795 (1987).
- [7] M. J. Savage, R. A. Malaney, and G. M. Fuller, Neutrino Oscillations and the Leptonic Charge of the Universe, *Astrophys. J.* **368**, 1 (1991).
- [8] J. Pantaleone, Dirac neutrinos in dense matter, *Phys. Rev. D* **46**, 510 (1992).
- [9] J. Pantaleone, Neutrino oscillations at high densities, *Phys. Lett. B* **287**, 128 (1992).
- [10] B. H. J. McKellar and M. J. Thomson, Oscillating neutrinos in the early universe, *Phys. Rev. D* **49**, 2710 (1994).

- [11] N. F. Bell, A. A. Rawlinson, and R. F. Sawyer, Speedup through entanglement: Many body effects in neutrino processes, *Phys. Lett. B* **573**, 86 (2003), [arXiv:hep-ph/0304082](#).
- [12] A. Friedland and C. Lunardini, Do many particle neutrino interactions cause a novel coherent effect?, *JHEP* **10**, 043, [arXiv:hep-ph/0307140](#).
- [13] R. F. Sawyer, ‘Classical’ instabilities and ‘quantum’ speed-up in the evolution of neutrino clouds (2004), [arXiv:hep-ph/0408265](#).
- [14] Y. Pehlivan, A. B. Balantekin, T. Kajino, and T. Yoshida, Invariants of Collective Neutrino Oscillations, *Phys. Rev. D* **84**, 065008 (2011), [arXiv:1105.1182 \[astro-ph.CO\]](#).
- [15] E. Rrapaj, Exact solution of multiangle quantum many-body collective neutrino-flavor oscillations, *Phys. Rev. C* **101**, 065805 (2020), [arXiv:1905.13335 \[hep-ph\]](#).
- [16] M. J. Cervia, A. V. Patwardhan, A. B. Balantekin, t. S. N. Coppersmith, and C. W. Johnson, Entanglement and collective flavor oscillations in a dense neutrino gas, *Phys. Rev. D* **100**, 083001 (2019), [arXiv:1908.03511 \[hep-ph\]](#).
- [17] A. Roggero, Entanglement and many-body effects in collective neutrino oscillations, *Phys. Rev. D* **104**, 103016 (2021), [arXiv:2102.10188 \[hep-ph\]](#).
- [18] B. Hall, A. Roggero, A. Baroni, and J. Carlson, Simulation of collective neutrino oscillations on a quantum computer, *Phys. Rev. D* **104**, 063009 (2021), [arXiv:2102.12556 \[quant-ph\]](#).
- [19] A. Roggero, Dynamical phase transitions in models of collective neutrino oscillations, *Phys. Rev. D* **104**, 123023 (2021), [arXiv:2103.11497 \[hep-ph\]](#).
- [20] K. Yeter-Aydeniz, S. Bangar, G. Siopsis, and R. C. Pooser, Collective neutrino oscillations on a quantum computer, *Quantum Inf. Process* **21**, 84 (2022), [arXiv:2104.03273 \[quant-ph\]](#).
- [21] A. V. Patwardhan, M. J. Cervia, and A. B. Balantekin, Spectral splits and entanglement entropy in collective neutrino oscillations, *Phys. Rev. D* **104**, 123035 (2021), [arXiv:2109.08995 \[hep-ph\]](#).
- [22] Z. Xiong, Many-body effects of collective neutrino oscillations, *Phys. Rev. D* **105**, 103002 (2022), [arXiv:2111.00437 \[astro-ph.HE\]](#).
- [23] J. D. Martin, A. Roggero, H. Duan, J. Carlson, and V. Cirigliano, Classical and quantum evolution in a simple coherent neutrino problem, *Phys. Rev. D* **105**, 083020 (2022), [arXiv:2112.12686 \[hep-ph\]](#).
- [24] M. J. Cervia, P. Siwach, A. V. Patwardhan, A. B. Balantekin, S. N. Coppersmith, and C. W. Johnson, Collective neutrino oscillations with tensor networks using a time-dependent variational principle, *Phys. Rev. D* **105**, 123025 (2022), [arXiv:2202.01865 \[hep-ph\]](#).
- [25] M. Illa and M. J. Savage, Basic elements for simulations of standard-model physics with quantum annealers: Multigrid and clock states, *Phys. Rev. A* **106**, 052605 (2022), [arXiv:2202.12340 \[quant-ph\]](#).
- [26] A. Roggero, E. Rrapaj, and Z. Xiong, Entanglement and correlations in fast collective neutrino flavor oscillations, *Phys. Rev. D* **106**, 043022 (2022), [arXiv:2203.02783 \[astro-ph.HE\]](#).
- [27] D. Lacroix, A. B. Balantekin, M. J. Cervia, A. V. Patwardhan, and P. Siwach, Role of non-Gaussian quantum fluctuations in neutrino entanglement, *Phys. Rev. D* **106**, 123006 (2022), [arXiv:2205.09384 \[nucl-th\]](#).
- [28] V. Amitrano, A. Roggero, P. Luchi, F. Turro, L. Vespucci, and F. Pederiva, Trapped-ion quantum simulation of collective neutrino oscillations, *Phys. Rev. D* **107**, 023007 (2023), [arXiv:2207.03189 \[quant-ph\]](#).
- [29] A. Wong and N. Christensen, Potential multiparticle entanglement measure, *Phys. Rev. A* **63**, 044301 (2001), [arXiv:quant-ph/0010052](#).
- [30] Quantinuum, <https://www.quantinuum.com/>, 2022.
- [31] B. Pontecorvo, Mesonium and anti-mesonium, *Sov. Phys. JETP* **6**, 429 (1957).
- [32] B. Pontecorvo, Inverse beta processes and nonconservation of lepton charge, *Sov. Phys. JETP* **7**, 172 (1958).
- [33] Z. Maki, M. Nakagawa, and S. Sakata, Remarks on the Unified Model of Elementary Particles, *Prog. Theor. Phys.* **28**, 870 (1962).
- [34] B. Pontecorvo, Neutrino Experiments and the Problem of Conservation of Leptonic Charge, *Sov. Phys. JETP* **26**, 984 (1968).
- [35] L. Wolfenstein, Neutrino Oscillations in Matter, *Phys. Rev. D* **17**, 2369 (1978).
- [36] S. P. Mikheyev and A. Y. Smirnov, Resonance Amplification of Oscillations in Matter and Spectroscopy of Solar Neutrinos, *Sov. J. Nucl. Phys.* **42**, 913 (1985).
- [37] I. Esteban, M. C. Gonzalez-Garcia, M. Maltoni, T. Schwetz, and A. Zhou, The fate of hints: updated global analysis of three-flavor neutrino oscillations, *J. High Energ. Phys.* **2020** (2020), 178, [arXiv:2007.14792 \[hep-ph\]](#).
- [38] A. B. Balantekin and G. M. Fuller, Constraints on neutrino mixing, *Phys. Lett. B* **471**, 195 (1999), [arXiv:hep-ph/9908465](#).
- [39] H.-Y. Huang, R. Kueng, and J. Preskill, Predicting many properties of a quantum system from very few measurements, *Nat. Phys.* **16**, 1050 (2020), [arXiv:2002.08953 \[quant-ph\]](#).
- [40] S. Hill and W. K. Wootters, Entanglement of a pair of quantum bits, *Phys. Rev. Lett.* **78**, 5022 (1997), [arXiv:quant-ph/9703041](#).
- [41] W. K. Wootters, Entanglement of formation of an arbitrary state of two qubits, *Phys. Rev. Lett.* **80**, 2245 (1998), [arXiv:quant-ph/9709029](#).
- [42] V. Coffman, J. Kundu, and W. K. Wootters, Distributed entanglement, *Phys. Rev. A* **61**, 052306 (2000), [arXiv:quant-ph/9907047](#).
- [43] X. Li and D. Li, Relationship between the n-tangle and the residual entanglement of even n qubits, *Quantum Inf. Comput.* **10**, 1018 (2010), [arXiv:1003.4774 \[quant-ph\]](#).
- [44] D. M. Greenberger, M. A. Horne, and A. Zeilinger, Going beyond bell’s theorem, in *Bell’s theorem, quantum theory and conceptions of the universe* (Springer, 1989) pp. 69–72, [arXiv:0712.0921 \[quant-ph\]](#).
- [45] D. Bouwmeester, J.-W. Pan, M. Daniell, H. Weinfurter, and A. Zeilinger, Observation of three photon Greenberger-Horne-Zeilinger entanglement, *Phys. Rev. Lett.* **82**, 1345 (1999), [arXiv:quant-ph/9810035](#).
- [46] W. Dur, G. Vidal, and J. I. Cirac, Three qubits can be entangled in two inequivalent ways, *Phys. Rev. A* **62**, 062314 (2000), [arXiv:quant-ph/0005115](#).
- [47] P. Hyllus, W. Laskowski, R. Krischek, C. Schwemmer, W. Wieczorek, H. Weinfurter, L. Pezzé, and A. Smerzi, Fisher information and multiparticle entanglement, *Phys. Rev. A* **85**, 022321 (2012), [arXiv:1006.4366 \[quant-ph\]](#).
- [48] G. Tóth, Multipartite entanglement and high-

- precision metrology, *Phys. Rev. A* **85**, 022322 (2012), [arXiv:1006.4368 \[quant-ph\]](#).
- [49] R. C. Farrell, I. A. Chernyshev, S. J. M. Powell, N. A. Zemel'skiy, M. Illa, and M. J. Savage, Preparations for quantum simulations of quantum chromodynamics in 1+1 dimensions. II. Single-baryon  $\beta$ -decay in real time, *Phys. Rev. D* **107**, 054513 (2023), [arXiv:2209.10781 \[quant-ph\]](#).
- [50] A. Barenco, C. H. Bennett, R. Cleve, D. P. DiVincenzo, N. Margolus, P. Shor, T. Sleator, J. Smolin, and H. Weinfurter, Elementary gates for quantum computation, *Phys. Rev. A* **52**, 3457 (1995), [arXiv:quant-ph/9503016](#).
- [51] F. Vatan and C. Williams, Optimal quantum circuits for general two-qubit gates, *Phys. Rev. A* **69**, 032315 (2004), [arXiv:quant-ph/0308006](#).
- [52] G. Vidal and C. M. Dawson, Universal quantum circuit for two-qubit transformations with three controlled-NOT gates, *Phys. Rev. A* **69**, 010301 (2004), [arXiv:quant-ph/0307177](#).
- [53] M. W. Coffey, R. Deiotte, and T. Semi, Comment on "Universal quantum circuit for two-qubit transformations with three controlled-NOT gates" and "Recognizing small-circuit structure in two-qubit operators", *Phys. Rev. A* **77**, 066301 (2008), [arXiv:quant-ph/0307177](#).
- [54] A. Paetznick and K. M. Svore, Repeat-Until-Success: Non-deterministic decomposition of single-qubit unitaries, *Quantum Info. Comput.* **14**, 1277 (2014), [arXiv:1311.1074 \[quant-ph\]](#).
- [55] A. G. Fowler, Constructing arbitrary Steane code single logical qubit fault-tolerant gates, *Quantum Info. Comput.* **11**, 867 (2011), [arXiv:quant-ph/0411206 \[quant-ph\]](#).
- [56] A. Bocharov and K. M. Svore, Resource-Optimal Single-Qubit Quantum Circuits, *Phys. Rev. Lett.* **109**, 190501 (2012), [arXiv:1206.3223 \[quant-ph\]](#).
- [57] V. Kliuchnikov, D. Maslov, and M. Mosca, Practical approximation of single-qubit unitaries by single-qubit quantum Clifford and T circuits, *IEEE Trans. Comput.* **65**, 161 (2016), [arXiv:1212.6964 \[quant-ph\]](#).
- [58] S. Sivarajah, S. Dilkes, A. Cowtan, W. Simmons, A. Edgington, and R. Duncan, `t|ket>`: a retargetable compiler for NISQ devices, *Quantum Sci. Technol.* **6**, 014003 (2020), [arXiv:2003.10611 \[quant-ph\]](#).
- [59] C. Cirstoiu, Z. Holmes, J. Iosue, L. Cincio, P. J. Coles, and A. Sornborger, Variational fast forwarding for quantum simulation beyond the coherence time, *npj Quantum Inf* **6**, 82 (2020), [arXiv:1910.04292 \[quant-ph\]](#).
- [60] N. Klco and M. J. Savage, Minimally entangled state preparation of localized wave functions on quantum computers, *Phys. Rev. A* **102**, 012612 (2020), [arXiv:1904.10440 \[quant-ph\]](#).
- [61] J. J. Wallman and J. Emerson, Noise tailoring for scalable quantum computation via randomized compiling, *Phys. Rev. A* **94**, 052325 (2016), [arXiv:1512.01098 \[quant-ph\]](#).
- [62] Urbanek, M. and Nachman, B. and Pascuzzi, V. R. and He, A. and Bauer, C. W. and de Jong, W. A., Mitigating depolarizing noise on quantum computers with noise-estimation circuits, *Phys. Rev. Lett.* **127**, 270502 (2021), [arXiv:2103.08591 \[quant-ph\]](#).
- [63] S. A. Rahman, R. Lewis, E. Mendicelli, and S. Powell, Self-mitigating Trotter circuits for SU(2) lattice gauge theory on a quantum computer, *Phys. Rev. D* **106**, 074502 (2022), [arXiv:2205.09247 \[hep-lat\]](#).
- [64] R. C. Farrell, I. A. Chernyshev, S. J. M. Powell, N. A. Zemel'skiy, M. Illa, and M. J. Savage, Preparations for quantum simulations of quantum chromodynamics in 1+1 dimensions. I. Axial gauge, *Phys. Rev. D* **107**, 054512 (2023), [arXiv:2207.01731 \[quant-ph\]](#).
- [65] N. Klco, J. R. Stryker, and M. J. Savage, SU(2) non-Abelian gauge field theory in one dimension on digital quantum computers, *Phys. Rev. D* **101**, 074512 (2020), [arXiv:1908.06935 \[quant-ph\]](#).
- [66] N. H. Nguyen, M. C. Tran, Y. Zhu, A. M. Green, C. H. Alderete, Z. Davoudi, and N. M. Linke, Digital Quantum Simulation of the Schwinger Model and Symmetry Protection with Trapped Ions, *PRX Quantum* **3**, 020324 (2022), [arXiv:2112.14262 \[quant-ph\]](#).
- [67] A. Barenco, A. Berthiaume, D. Deutsch, A. Ekert, R. Jozsa, and C. Macchiavello, Stabilization of quantum computations by symmetrization, *SIAM Journal on Computing* **26**, 1541 (1997), [arXiv:quant-ph/9604028](#).
- [68] H. Buhrman, R. Cleve, J. Watrous, and R. de Wolf, Quantum fingerprinting, *Phys. Rev. Lett.* **87**, 167902 (2001), [arXiv:quant-ph/0102001](#).
- [69] J. L. Beckey, N. Gigena, P. J. Coles, and M. Cerezo, Computable and operationally meaningful multipartite entanglement measures, *Phys. Rev. Lett.* **127**, 140501 (2021), [arXiv:2104.06923 \[quant-ph\]](#).
- [70] Wolfram Research, Inc., *Mathematica*, Version 13.0.1 (2022), Champaign, IL.
- [71] G. Van Rossum and F. L. Drake, *Python 3 Reference Manual* (CreateSpace, Scotts Valley, CA, 2009).
- [72] J. D. Hunter, Matplotlib: A 2D graphics environment, *Comput. Sci. Eng.* **9**, 90 (2007).
- [73] F. Pérez and B. E. Granger, IPython: a System for Interactive Scientific Computing, *Comput. Sci. Eng.* **9**, 21 (2007).
- [74] Anaconda Inc., *Anaconda Software Distribution*, Vers. 2-2.4.0 (2020).
- [75] J. Bezanson, A. Edelman, S. Karpinski, and V. B. Shah, Julia: A fresh approach to numerical computing, *SIAM Review* **59**, 65 (2017).
- [76] A. Croy *et al.*, Expokit.jl: Julia implementations of Expokit, <https://github.com/acroy/Expokit.jl> (2018).
- [77] R. B. Sidje, Expokit: A Software Package for Computing Matrix Exponentials, *ACM Trans. Math. Softw.* **24**, 130 (1998).
- [78] M. Treinish, J. Gambetta, P. Nation, qiskit bot, P. Kassebaum, D. M. Rodríguez, S. de la Puente González, S. Hu, K. Krsulich, J. Garrison, L. Zdanski, J. Lishman, J. Yu, J. Gacon, D. McKay, J. Gomez, L. Capelluto, Travis-S-IBM, M. Marques, A. Panigrahi, lerongil, R. I. Rahman, S. Wood, L. Bello, T. Itoko, C. J. Wood, D. Singh, Drew, E. Arbel, and J. Schwarm, *Qiskit/qiskit: Qiskit 0.36.2* (2022).

**SUPPLEMENTARY MATERIAL**  
**MULTI-NEUTRINO ENTANGLEMENT AND CORRELATIONS IN DENSE NEUTRINO SYSTEMS**

This supplementary material contains additional figures and the tabulated results obtained with quantum simulations using Quantinuum’s 20 trapped-ion quantum computer H1-1, its noisy emulator H1-1E, and other classical simulations, used to produce the figures. In the legend of the figures, “Exact” results are obtained by computing the exponentiation of the Hamiltonian with `Mathematica` [70], except for the results for the  $n$ -tuple in Fig. 5, where `Julia` [75] was used (with its `Expokit` package [76]). The “Trotter” results were obtained with `Mathematica` also, by first identifying the different terms in the Hamiltonian that can be implemented together (mainly, those shown in Eqs. (7) and (8)), exponentiating them separately, and multiplying them in the order used in the quantum circuits (as a check, this was compared with the results obtained with the `qiskit` noiseless simulator [78] using the quantum circuits run on H1-1).

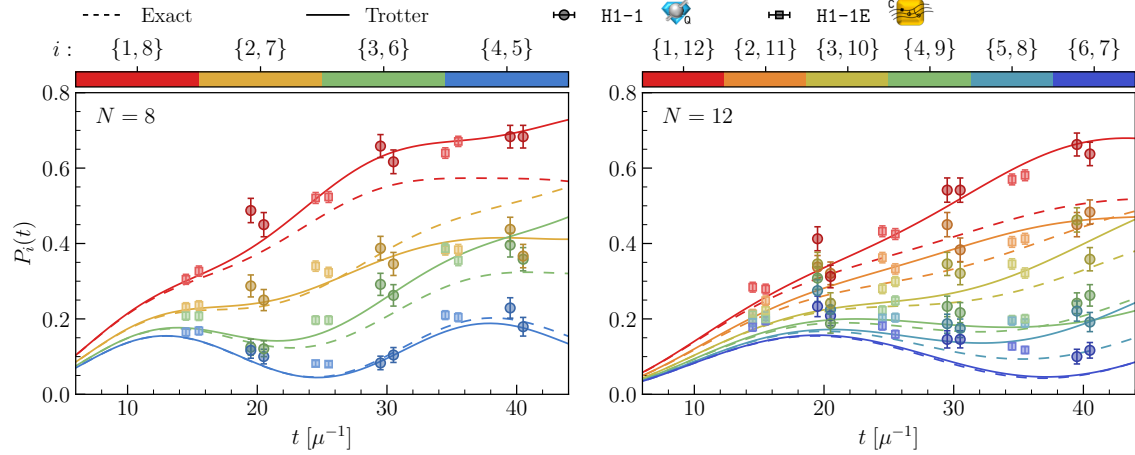


FIG. S1. Flavor inversion probabilities for systems with  $N = 8$  (left) and  $N = 12$  (right) neutrinos. The lines show the single-step Trotter (continuous) and exact (dashed) simulations, and the points show the results from H1-1 (dark circles, using 240 shots) and H1-1E (light squares, using 1200 shots).

		$P_1(t)$		$P_8(t)$				$P_2(t)$		$P_7(t)$			
$t$		H1-1	H1-1E	H1-1	H1-1E	1-T		$t$	H1-1	H1-1E	H1-1	H1-1E	1-T
15	—	—	0.305(13)	—	0.327(14)	0.308		15	—	0.231(12)	—	0.236(12)	0.226
20	0.488(32)	—	0.450(32)	—	—	0.399		20	0.287(29)	—	0.250(28)	—	0.242
25	—	0.521(14)	—	0.523(14)	—	0.532		25	—	0.340(14)	—	0.323(14)	0.291
30	0.658(30)	—	0.617(31)	—	—	0.637		30	0.387(31)	—	0.346(31)	—	0.361
35	—	0.640(14)	—	0.671(14)	—	0.671		35	—	0.383(14)	—	0.383(14)	0.406
40	0.683(30)	—	0.683(30)	—	—	0.694		40	0.438(32)	—	0.367(31)	—	0.415

		$P_3(t)$		$P_6(t)$				$P_4(t)$		$P_5(t)$			
$t$		H1-1	H1-1E	H1-1	H1-1E	1-T		$t$	H1-1	H1-1E	H1-1	H1-1E	1-T
15	—	—	0.208(12)	—	0.208(12)	0.175		15	—	0.165(11)	—	0.168(11)	0.146
20	0.125(21)	—	0.121(21)	—	—	0.145		20	0.117(21)	—	0.100(19)	—	0.081
25	—	0.197(11)	—	0.197(12)	—	0.163		25	—	0.082(8)	—	0.080(8)	0.045
30	0.292(29)	—	0.262(28)	—	—	0.258		30	0.083(18)	—	0.104(20)	—	0.095
35	—	0.387(14)	—	0.355(14)	—	0.360		35	—	0.210(12)	—	0.204(12)	0.172
40	0.396(32)	—	0.358(31)	—	—	0.424		40	0.229(27)	—	0.179(25)	—	0.180

TABLE S1. Results from Fig. S1 showing the inversion probability  $P_i(t)$  for the  $N = 8$  neutrino system. The results computed using H1-1 were obtained using 240 shots, and those using H1-1E with 1200 shots. The column labeled “1-T” is the exact value using a single Trotter step.



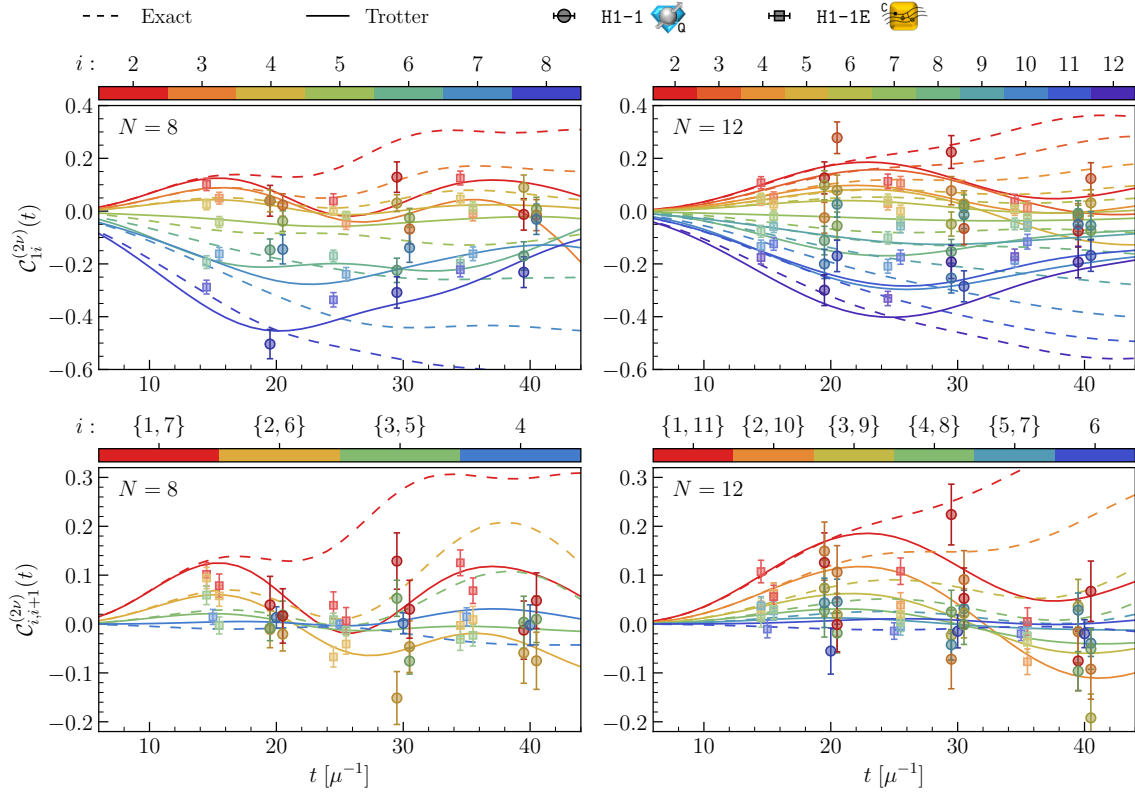


FIG. S2. Two-body correlations for systems with  $N = 8$  (left) and  $N = 12$  (right) neutrinos. The lines show the single-step Trotter (continuous) and exact (dashed) simulations, and the points show the results from H1-1 (dark circles, using 240 shots) and H1-1E (light squares, using 1200 shots).

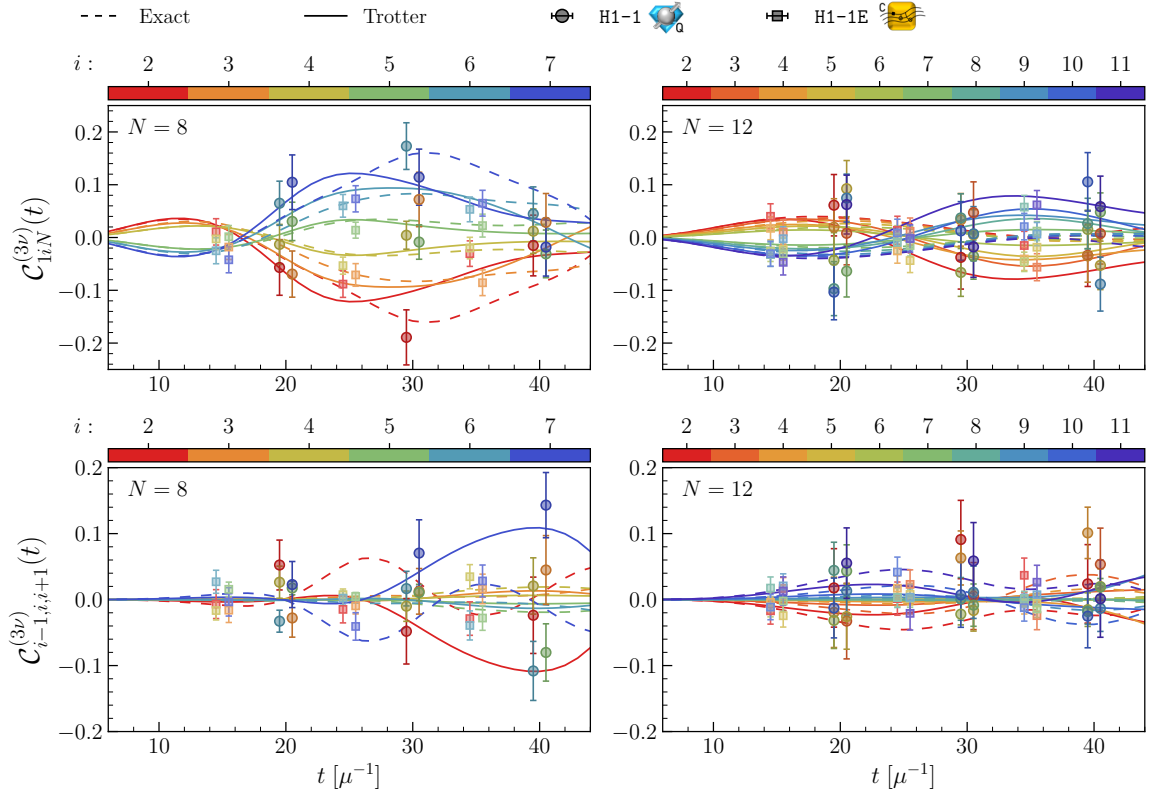


FIG. S3. Three-body correlations for systems with  $N = 8$  (left) and  $N = 12$  (right) neutrinos. The lines show the single-step Trotter (continuous) and exact (dashed) simulations, and the points show the results from H1-1 (dark circles, using 240 shots) and H1-1E (light squares, using 1200 shots).

		$P_1(t)$		$P_{12}(t)$				$P_2(t)$		$P_{11}(t)$					
$t$	H1-1	H1-1E	H1-1	H1-1E	1-T	$t$	H1-1	H1-1E	H1-1	H1-1E	1-T	$t$	H1-1	H1-1E	1-T
15	—	0.284(13)	—	0.279(13)	0.248	15	—	0.213(12)	—	0.248(12)	0.212	15	—	0.200(12)	0.161
20	0.413(32)	—	0.313(30)	—	0.336	20	0.338(31)	—	0.321(30)	—	0.282	20	0.308(30)	—	0.196
25	—	0.432(14)	—	0.425(14)	0.416	25	—	0.362(14)	—	0.333(14)	0.333	25	—	0.223(12)	0.197
30	0.542(32)	—	0.542(32)	—	0.508	30	0.450(32)	—	0.383(31)	—	0.385	30	0.233(27)	—	0.184
35	—	0.570(14)	—	0.581(14)	0.605	35	—	0.404(14)	—	0.413(14)	0.433	35	—	0.198(11)	0.178
40	0.663(30)	—	0.638(31)	—	0.668	40	0.450(32)	—	0.483(32)	—	0.462	40	0.242(28)	—	0.193

		$P_3(t)$		$P_{10}(t)$				$P_4(t)$		$P_9(t)$					
$t$	H1-1	H1-1E	H1-1	H1-1E	1-T	$t$	H1-1	H1-1E	H1-1	H1-1E	1-T	$t$	H1-1	H1-1E	1-T
15	—	0.198(11)	—	0.223(12)	0.178	15	—	0.211(12)	—	0.200(12)	0.161	15	—	0.200(12)	0.161
20	0.346(31)	—	0.242(28)	—	0.224	20	0.308(30)	—	0.188(25)	—	0.196	20	0.308(30)	—	0.196
25	—	0.280(13)	—	0.299(13)	0.245	25	—	0.223(12)	—	0.248(12)	0.197	25	—	0.223(12)	0.197
30	0.346(31)	—	0.321(30)	—	0.269	30	0.233(27)	—	0.217(27)	—	0.184	30	0.233(27)	—	0.184
35	—	0.346(14)	—	0.322(14)	0.321	35	—	0.198(11)	—	0.200(12)	0.178	35	—	0.198(11)	0.178
40	0.463(32)	—	0.358(31)	—	0.399	40	0.242(28)	—	0.262(28)	—	0.193	40	0.242(28)	—	0.193

		$P_5(t)$		$P_8(t)$				$P_6(t)$		$P_7(t)$					
$t$	H1-1	H1-1E	H1-1	H1-1E	1-T	$t$	H1-1	H1-1E	H1-1	H1-1E	1-T	$t$	H1-1	H1-1E	1-T
15	—	0.191(11)	—	0.208(12)	0.146	15	—	0.178(11)	—	0.196(11)	0.138	15	—	0.196(11)	0.138
20	0.275(29)	—	0.225(27)	—	0.172	20	0.233(27)	—	0.208(26)	—	0.157	20	0.233(27)	—	0.157
25	—	0.203(12)	—	0.203(12)	0.160	25	—	0.182(11)	—	0.159(11)	0.132	25	—	0.182(11)	0.132
30	0.187(25)	—	0.175(25)	—	0.139	30	0.146(23)	—	0.146(23)	—	0.085	30	0.146(23)	—	0.085
35	—	0.195(11)	—	0.189(11)	0.142	35	—	0.127(10)	—	0.118(9)	0.050	35	—	0.127(10)	0.050
40	0.221(27)	—	0.192(25)	—	0.186	40	0.100(19)	—	0.117(21)	—	0.053	40	0.100(19)	—	0.053

TABLE S2. Results from Fig. S1 showing the inversion probability  $P_i(t)$  for the  $N = 12$  neutrino system. The results computed using H1-1 were obtained using 240 shots, and those using H1-1E with 1200 shots. The column labeled “1-T” is the exact value using a single Trotter step.

		$\mathcal{C}_{1,2}^{(2\nu)}(t)$				$\mathcal{C}_{1,3}^{(2\nu)}(t)$				$\mathcal{C}_{1,4}^{(2\nu)}(t)$					
$t$	H1-1	H1-1E	1-T	$t$	H1-1	H1-1E	1-T	$t$	H1-1	H1-1E	1-T	$t$	H1-1	H1-1E	1-T
15	—	0.102(24)	0.125	15	—	0.049(22)	0.088	15	—	0.025(20)	0.043	15	—	0.025(20)	0.043
20	0.039(58)	—	0.071	20	0.023(43)	—	0.050	20	0.039(41)	—	0.019	20	0.039(41)	—	0.019
25	—	0.038(27)	-0.017	25	—	-0.046(23)	-0.033	25	—	0.000(16)	-0.013	25	—	0.000(16)	-0.013
30	0.129(58)	—	0.033	30	-0.068(57)	—	-0.016	30	0.030(32)	—	0.003	30	0.030(32)	—	0.003
35	—	0.125(26)	0.111	35	—	-0.010(27)	0.043	35	—	0.046(22)	0.023	35	—	0.046(22)	0.023
40	-0.012(60)	—	0.105	40	-0.015(59)	—	-0.022	40	0.090(47)	—	0.021	40	0.090(47)	—	0.021

		$\mathcal{C}_{1,5}^{(2\nu)}(t)$				$\mathcal{C}_{1,6}^{(2\nu)}(t)$				$\mathcal{C}_{1,7}^{(2\nu)}(t)$					
$t$	H1-1	H1-1E	1-T	$t$	H1-1	H1-1E	1-T	$t$	H1-1	H1-1E	1-T	$t$	H1-1	H1-1E	1-T
15	—	-0.041(21)	-0.030	15	—	-0.193(24)	-0.187	15	—	-0.162(24)	-0.188	15	—	-0.162(24)	-0.188
20	-0.038(39)	—	-0.050	20	-0.147(41)	—	-0.211	20	-0.145(55)	—	-0.264	20	-0.145(55)	—	-0.264
25	—	-0.017(16)	-0.058	25	—	-0.170(22)	-0.199	25	—	-0.239(26)	-0.268	25	—	-0.239(26)	-0.268
30	-0.025(36)	—	-0.045	30	-0.224(46)	—	-0.220	30	-0.139(55)	—	-0.216	30	-0.139(55)	—	-0.216
35	—	0.013(22)	-0.029	35	—	-0.198(25)	-0.216	35	—	-0.162(26)	-0.165	35	—	-0.162(26)	-0.165
40	0.006(46)	—	-0.021	40	-0.170(54)	—	-0.147	40	-0.031(57)	—	-0.130	40	-0.031(57)	—	-0.130

		$\mathcal{C}_{1,8}^{(2\nu)}(t)$	
$t$	H1-1	H1-1E	1-T
15	—	-0.288(26)	-0.378
20	-0.504(56)	—	-0.454
25	—	-0.336(27)	-0.409
30	-0.308(59)	—	-0.346
35	—	-0.222(27)	-0.279
40	-0.231(58)	—	-0.174

TABLE S3. Results from Fig. S2 showing the two-body correlation  $\mathcal{C}_{1,i}^{(2\nu)}(t)$  for the  $N = 8$  neutrino system. The results computed using H1-1 were obtained using 240 shots, and those using H1-1E with 1200 shots. The column labeled “1-T” is the exact value using a single Trotter step.

$\mathcal{C}_{1,2}^{(2\nu)}(t)$						$\mathcal{C}_{7,8}^{(2\nu)}(t)$					
$t$	H1-1	H1-1E	H1-1	H1-1E	1-T	$t$	H1-1	H1-1E	H1-1	H1-1E	1-T
15	—	0.102(24)	—	0.079(24)	0.125	15	—	0.094(22)	—	0.058(21)	0.060
20	0.039(58)	—	0.017(56)	—	0.071	20	-0.011(38)	—	-0.021(34)	—	0.023
25	—	0.038(27)	—	0.007(27)	-0.017	25	—	-0.067(21)	—	-0.041(21)	-0.053
30	0.129(58)	—	0.030(59)	—	0.033	30	-0.151(54)	—	-0.046(53)	—	-0.053
35	—	0.125(26)	—	0.068(26)	0.111	35	—	-0.003(27)	—	0.009(27)	-0.020
40	-0.012(60)	—	0.048(57)	—	0.105	40	-0.059(62)	—	-0.075(58)	—	-0.044

$\mathcal{C}_{3,4}^{(2\nu)}(t)$						$\mathcal{C}_{5,6}^{(2\nu)}(t)$						$\mathcal{C}_{4,5}^{(2\nu)}(t)$					
$t$	H1-1	H1-1E	H1-1	H1-1E	1-T	$t$	H1-1	H1-1E	H1-1	H1-1E	1-T	$t$	H1-1	H1-1E	H1-1	H1-1E	1-T
15	—	0.059(19)	—	-0.003(17)	0.021	15	—	0.015(15)	—	0.004	15	—	0.015(15)	—	0.004		
20	-0.008(26)	—	0.018(29)	—	0.008	20	0.013(22)	—	—	0.004	20	0.013(22)	—	—	0.004		
25	—	0.009(13)	—	-0.013(11)	-0.012	25	—	-0.001(9)	—	-0.003	25	—	-0.001(9)	—	-0.003		
30	0.053(37)	—	-0.076(27)	—	-0.010	30	0.001(21)	—	—	0.007	30	0.001(21)	—	—	0.007		
35	—	-0.031(23)	—	-0.023(22)	-0.005	35	—	0.015(19)	—	0.028	35	—	0.015(19)	—	0.028		
40	0.004(53)	—	0.010(48)	—	-0.010	40	-0.002(42)	—	—	0.026	40	-0.002(42)	—	—	0.026		

TABLE S4. Results from Fig. S2 showing the two-body correlation  $\mathcal{C}_{i,i+1}^{(2\nu)}(t)$  for the  $N = 8$  neutrino system. The results computed using H1-1 were obtained using 240 shots, and those using H1-1E with 1200 shots. The column labeled “1-T” is the exact value using a single Trotter step.

$\mathcal{C}_{1,2,8}^{(3\nu)}(t)$				$\mathcal{C}_{1,3,8}^{(3\nu)}(t)$				$\mathcal{C}_{1,4,8}^{(3\nu)}(t)$			
$t$	H1-1	H1-1E	1-T	$t$	H1-1	H1-1E	1-T	$t$	H1-1	H1-1E	1-T
15	—	0.011(25)	0.019	15	—	-0.018(24)	0.018	15	—	-0.003(20)	0.020
20	-0.057(53)	—	-0.068	20	-0.069(44)	—	-0.040	20	-0.013(38)	—	-0.010
25	—	-0.088(25)	-0.122	25	—	-0.071(21)	-0.089	25	—	-0.053(16)	-0.034
30	-0.189(52)	—	-0.102	30	0.072(52)	—	-0.093	30	0.004(26)	—	-0.024
35	—	-0.031(24)	-0.062	35	—	-0.086(24)	-0.072	35	—	-0.020(20)	-0.012
40	-0.015(58)	—	-0.034	40	0.029(54)	—	-0.025	40	0.012(42)	—	-0.008

$\mathcal{C}_{1,5,8}^{(3\nu)}(t)$				$\mathcal{C}_{1,6,8}^{(3\nu)}(t)$				$\mathcal{C}_{1,7,8}^{(3\nu)}(t)$			
$t$	H1-1	H1-1E	1-T	$t$	H1-1	H1-1E	1-T	$t$	H1-1	H1-1E	1-T
15	—	0.001(21)	-0.020	15	—	-0.025(25)	-0.018	15	—	-0.042(25)	-0.019
20	0.031(36)	—	0.010	20	0.065(42)	—	0.040	20	0.105(52)	—	0.068
25	—	0.014(15)	0.034	25	—	0.060(22)	0.089	25	—	0.073(25)	0.122
30	-0.009(33)	—	0.024	30	0.173(44)	—	0.093	30	0.114(54)	—	0.102
35	—	0.023(22)	0.012	35	—	0.053(23)	0.072	35	—	0.065(24)	0.062
40	-0.031(45)	—	0.008	40	0.045(51)	—	0.025	40	-0.018(55)	—	0.034

TABLE S5. Results from Fig. S3 showing the three-body correlation  $\mathcal{C}_{i,iN}^{(3\nu)}(t)$  for the  $N = 8$  neutrino system. The results computed using H1-1 were obtained using 240 shots, and those using H1-1E with 1200 shots. The column labeled “1-T” is the exact value using a single Trotter step.

$\mathcal{C}_{1,2,3}^{(3\nu)}(t)$				$\mathcal{C}_{2,3,4}^{(3\nu)}(t)$				$\mathcal{C}_{3,4,5}^{(3\nu)}(t)$			
$t$	H1-1	H1-1E	1-T	$t$	H1-1	H1-1E	1-T	$t$	H1-1	H1-1E	1-T
15	—	-0.007(22)	-0.003	15	—	-0.016(19)	0.001	15	—	-0.017(14)	0.0005
20	0.052(38)	—	0.001	20	-0.028(29)	—	0.001	20	0.026(24)	—	0.001
25	—	-0.015(20)	0.004	25	—	-0.009(12)	-0.001	25	—	0.007(9)	0.0001
30	-0.048(50)	—	-0.036	30	0.013(35)	—	0.001	30	-0.010(23)	—	0.002
35	—	-0.029(25)	-0.088	35	—	0.016(22)	0.009	35	—	0.035(18)	0.005
40	-0.024(58)	—	-0.109	40	0.045(52)	—	0.013	40	0.021(43)	—	0.006

$\mathcal{C}_{4,5,6}^{(3\nu)}(t)$				$\mathcal{C}_{5,6,7}^{(3\nu)}(t)$				$\mathcal{C}_{6,7,8}^{(3\nu)}(t)$			
$t$	H1-1	H1-1E	1-T	$t$	H1-1	H1-1E	1-T	$t$	H1-1	H1-1E	1-T
15	—	0.016(11)	-0.0005	15	—	0.027(17)	-0.001	15	—	-0.003(21)	0.003
20	0.018(10)	—	-0.001	20	-0.033(17)	—	-0.001	20	0.023(35)	—	-0.001
25	—	0.005(6)	-0.0001	25	—	0.002(10)	0.001	25	—	-0.041(21)	-0.004
30	0.011(12)	—	-0.002	30	0.017(26)	—	-0.001	30	0.070(50)	—	0.036
35	—	-0.028(19)	-0.005	35	—	-0.039(22)	-0.009	35	—	0.028(24)	0.088
40	-0.080(43)	—	-0.006	40	-0.108(45)	—	-0.013	40	0.143(49)	—	0.109

TABLE S6. Results from Fig. S3 showing the three-body correlation  $\mathcal{C}_{i-1,i,i+1}^{(3\nu)}(t)$  for the  $N = 8$  neutrino system. The results computed using H1-1 were obtained using 240 shots, and those using H1-1E with 1200 shots. The column labeled “1-T” is the exact value using a single Trotter step.

$\mathcal{C}_{1,2}^{(2\nu)}(t)$				$\mathcal{C}_{1,3}^{(2\nu)}(t)$				$\mathcal{C}_{1,4}^{(2\nu)}(t)$			
$t$	H1-1	H1-1E	1-T	$t$	H1-1	H1-1E	1-T	$t$	H1-1	H1-1E	1-T
15	—	0.107(23)	0.107	15	—	0.051(22)	0.084	15	—	0.044(22)	0.060
20	0.126(61)	—	0.173	20	0.278(60)	—	0.141	20	-0.025(58)	—	0.094
25	—	0.113(28)	0.179	25	—	0.105(26)	0.155	25	—	0.028(24)	0.088
30	0.224(62)	—	0.119	30	-0.066(61)	—	0.111	30	0.077(53)	—	0.043
35	—	0.035(28)	0.057	35	—	0.012(27)	0.040	35	—	0.006(23)	-0.001
40	-0.076(61)	—	0.054	40	0.124(60)	—	-0.007	40	-0.024(53)	—	-0.003

$\mathcal{C}_{1,5}^{(2\nu)}(t)$				$\mathcal{C}_{1,6}^{(2\nu)}(t)$				$\mathcal{C}_{1,7}^{(2\nu)}(t)$			
$t$	H1-1	H1-1E	1-T	$t$	H1-1	H1-1E	1-T	$t$	H1-1	H1-1E	1-T
15	—	0.026(21)	0.045	15	—	0.047(21)	0.027	15	—	-0.021(21)	-0.014
20	0.079(57)	—	0.076	20	0.098(55)	—	0.039	20	-0.056(52)	—	-0.022
25	—	0.000(23)	0.077	25	—	0.042(22)	0.034	25	—	-0.035(21)	-0.030
30	0.027(50)	—	0.031	30	-0.049(46)	—	0.013	30	0.016(45)	—	-0.036
35	—	-0.051(23)	-0.048	35	—	0.009(19)	-0.004	35	—	-0.025(18)	-0.036
40	0.031(50)	—	-0.112	40	-0.015(37)	—	-0.005	40	-0.074(35)	—	-0.033

$\mathcal{C}_{1,8}^{(2\nu)}(t)$				$\mathcal{C}_{1,9}^{(2\nu)}(t)$				$\mathcal{C}_{1,10}^{(2\nu)}(t)$			
$t$	H1-1	H1-1E	1-T	$t$	H1-1	H1-1E	1-T	$t$	H1-1	H1-1E	1-T
15	—	-0.076(23)	-0.095	15	—	-0.059(22)	-0.061	15	—	-0.134(24)	-0.162
20	-0.111(54)	—	-0.151	20	0.026(49)	—	-0.094	20	-0.200(55)	—	-0.253
25	—	-0.101(23)	-0.169	25	—	-0.057(25)	-0.119	25	—	-0.209(26)	-0.296
30	-0.153(46)	—	-0.144	30	-0.014(53)	—	-0.126	30	-0.254(56)	—	-0.281
35	—	-0.049(22)	-0.108	35	—	-0.054(22)	-0.114	35	—	-0.186(26)	-0.238
40	-0.009(48)	—	-0.084	40	-0.054(52)	—	-0.098	40	-0.050(58)	—	-0.197

$\mathcal{C}_{1,11}^{(2\nu)}(t)$				$\mathcal{C}_{1,12}^{(2\nu)}(t)$			
$t$	H1-1	H1-1E	1-T	$t$	H1-1	H1-1E	1-T
15	—	-0.124(24)	-0.160	15	—	-0.176(25)	-0.246
20	-0.170(59)	—	-0.241	20	-0.300(58)	—	-0.360
25	—	-0.174(27)	-0.283	25	—	-0.331(27)	-0.402
30	-0.285(59)	—	-0.264	30	-0.192(63)	—	-0.359
35	—	-0.116(28)	-0.208	35	—	-0.172(28)	-0.278
40	-0.169(60)	—	-0.166	40	-0.193(60)	—	-0.218

TABLE S7. Results from Fig. S2 showing the two-body correlation  $\mathcal{C}_{i_i}^{(2\nu)}(t)$  for the  $N = 12$  neutrino system. The results computed using H1-1 were obtained using 240 shots, and those using H1-1E with 1200 shots. The column labeled “1-T” is the exact value using a single Trotter step.

$C_{1,2}^{(2\nu)}(t)$						$C_{11,12}^{(2\nu)}(t)$					$C_{2,3}^{(2\nu)}(t)$						$C_{10,11}^{(2\nu)}(t)$						
$t$	H1-1	H1-1E	H1-1	H1-1E	1-T	$t$	H1-1	H1-1E	H1-1	H1-1E	1-T	$t$	H1-1	H1-1E	H1-1	H1-1E	1-T	$t$	H1-1	H1-1E	H1-1	H1-1E	1-T
15	—	0.107(23)	—	0.056(23)	0.107	15	—	0.027(20)	—	0.062(22)	0.068	15	—	0.027(20)	—	0.030(20)	0.020	15	—	0.012(19)	—	0.030(20)	0.020
20	0.126(61)	—	-0.001(56)	—	0.173	20	0.149(59)	—	0.106(54)	—	0.111	20	0.027(54)	—	-0.019(41)	—	0.031	20	0.027(54)	—	-0.019(41)	—	0.031
25	—	0.113(28)	—	0.108(27)	0.179	25	—	0.051(25)	—	0.039(25)	0.108	25	—	0.013(20)	—	0.005(20)	0.024	25	—	0.013(20)	—	0.005(20)	0.024
30	0.224(62)	—	0.052(62)	—	0.119	30	-0.072(61)	—	0.091(59)	—	0.041	30	0.025(44)	—	-0.002(40)	—	-0.0002	30	0.025(44)	—	-0.002(40)	—	-0.0002
35	—	0.035(28)	—	0.005(28)	0.057	35	—	-0.082(27)	—	-0.077(26)	-0.054	35	—	-0.007(18)	—	-0.025(17)	-0.027	35	—	-0.007(18)	—	-0.025(17)	-0.027
40	-0.076(61)	—	0.067(62)	—	0.054	40	-0.016(64)	—	-0.092(61)	—	-0.109	40	-0.096(40)	—	-0.051(42)	—	-0.040	40	-0.096(40)	—	-0.051(42)	—	-0.040

$C_{3,4}^{(2\nu)}(t)$						$C_{9,10}^{(2\nu)}(t)$					$C_{4,5}^{(2\nu)}(t)$						$C_{8,9}^{(2\nu)}(t)$						
$t$	H1-1	H1-1E	H1-1	H1-1E	1-T	$t$	H1-1	H1-1E	H1-1	H1-1E	1-T	$t$	H1-1	H1-1E	H1-1	H1-1E	1-T	$t$	H1-1	H1-1E	H1-1	H1-1E	1-T
15	—	0.033(20)	—	0.062(21)	0.038	15	—	0.019(44)	—	0.060	15	—	0.012(19)	—	0.030(20)	0.020	15	—	0.012(19)	—	0.030(20)	0.020	
20	0.073(58)	—	0.019(44)	—	0.060	20	0.073(58)	—	0.019(44)	—	0.060	20	0.027(54)	—	-0.019(41)	—	0.031	20	0.027(54)	—	-0.019(41)	—	0.031
25	—	0.024(22)	—	0.020(23)	0.054	25	—	0.020(23)	—	0.054	25	—	0.013(20)	—	0.005(20)	0.024	25	—	0.013(20)	—	0.005(20)	0.024	
30	-0.023(51)	—	0.022(50)	—	0.012	30	-0.023(51)	—	0.022(50)	—	0.012	30	0.025(44)	—	-0.002(40)	—	-0.0002	30	0.025(44)	—	-0.002(40)	—	-0.0002
35	—	-0.023(21)	—	-0.037(21)	-0.039	35	—	-0.037(21)	—	-0.039	35	—	-0.007(18)	—	-0.025(17)	-0.027	35	—	-0.007(18)	—	-0.025(17)	-0.027	
40	0.036(55)	—	-0.192(49)	—	-0.060	40	0.036(55)	—	-0.192(49)	—	-0.060	40	-0.096(40)	—	-0.051(42)	—	-0.040	40	-0.096(40)	—	-0.051(42)	—	-0.040

$C_{5,6}^{(2\nu)}(t)$						$C_{7,8}^{(2\nu)}(t)$					$C_{6,7}^{(2\nu)}(t)$									
$t$	H1-1	H1-1E	H1-1	H1-1E	1-T	$t$	H1-1	H1-1E	H1-1	H1-1E	1-T	$t$	H1-1	H1-1E	H1-1	H1-1E	1-T			
15	—	0.037(19)	—	0.027(19)	0.009	15	—	0.046(46)	—	0.013	15	—	-0.010(18)	—	0.002	15	—	-0.010(18)	—	0.002
20	0.043(50)	—	0.046(46)	—	0.013	20	0.043(50)	—	0.046(46)	—	0.013	20	-0.055(47)	—	0.007	20	-0.055(47)	—	0.007	
25	—	0.019(18)	—	-0.006(17)	0.008	25	—	-0.006(17)	—	0.008	25	—	-0.014(17)	—	0.011	25	—	-0.014(17)	—	0.011
30	-0.043(31)	—	0.031(38)	—	-0.001	30	-0.043(31)	—	0.031(38)	—	-0.001	30	-0.015(34)	—	0.008	30	-0.015(34)	—	0.008	
35	—	0.011(16)	—	-0.002(14)	-0.008	35	—	-0.002(14)	—	-0.008	35	—	-0.020(14)	—	0.001	35	—	-0.020(14)	—	0.001
40	0.028(35)	—	-0.039(27)	—	-0.011	40	0.028(35)	—	-0.039(27)	—	-0.011	40	-0.020(29)	—	0.0005	40	-0.020(29)	—	0.0005	

TABLE S8. Results from Fig. S2 showing the two-body correlation  $C_{i,i+1}^{(2\nu)}(t)$  for the  $N = 12$  neutrino system. The results computed using H1-1 were obtained using 240 shots, and those using H1-1E with 1200 shots. The column labeled “1-T” is the exact value using a single Trotter step.

$\mathcal{C}_{1,2,12}^{(3\nu)}(t)$				$\mathcal{C}_{1,3,12}^{(3\nu)}(t)$				$\mathcal{C}_{1,4,12}^{(3\nu)}(t)$			
$t$	H1-1	H1-1E	1-T	$t$	H1-1	H1-1E	1-T	$t$	H1-1	H1-1E	1-T
15	—	0.040(24)	0.034	15	—	0.010(23)	0.032	15	—	0.017(22)	0.024
20	0.061(58)	—	0.020	20	0.008(60)	—	0.031	20	0.019(54)	—	0.019
25	—	0.014(26)	-0.025	25	—	0.012(25)	0.003	25	—	-0.025(23)	-0.005
30	-0.038(60)	—	-0.069	30	0.047(58)	—	-0.036	30	0.034(50)	—	-0.034
35	—	-0.015(27)	-0.078	35	—	-0.056(26)	-0.054	35	—	-0.041(22)	-0.042
40	-0.034(59)	—	-0.062	40	0.007(58)	—	-0.039	40	-0.035(50)	—	-0.033

$\mathcal{C}_{1,5,12}^{(3\nu)}(t)$				$\mathcal{C}_{1,6,12}^{(3\nu)}(t)$				$\mathcal{C}_{1,7,12}^{(3\nu)}(t)$			
$t$	H1-1	H1-1E	1-T	$t$	H1-1	H1-1E	1-T	$t$	H1-1	H1-1E	1-T
15	—	-0.022(21)	0.020	15	—	-0.026(20)	0.013	15	—	-0.031(21)	-0.013
20	0.094(53)	—	0.020	20	-0.043(53)	—	0.013	20	-0.064(49)	—	-0.013
25	—	-0.044(23)	0.040	25	—	0.001(21)	0.003	25	—	-0.015(20)	-0.003
30	0.005(47)	—	-0.022	30	-0.066(45)	—	-0.009	30	-0.035(44)	—	0.009
35	—	-0.018(21)	-0.036	35	—	-0.046(18)	-0.015	35	—	0.012(18)	0.015
40	-0.053(46)	—	-0.025	40	0.015(36)	—	-0.013	40	0.048(36)	—	0.013

$\mathcal{C}_{1,8,12}^{(3\nu)}(t)$				$\mathcal{C}_{1,9,12}^{(3\nu)}(t)$				$\mathcal{C}_{1,10,12}^{(3\nu)}(t)$			
$t$	H1-1	H1-1E	1-T	$t$	H1-1	H1-1E	1-T	$t$	H1-1	H1-1E	1-T
15	—	-0.032(22)	-0.020	15	—	-0.002(22)	-0.024	15	—	-0.031(24)	-0.032
20	-0.097(51)	—	-0.020	20	0.075(45)	—	-0.019	20	-0.103(52)	—	-0.031
25	—	-0.009(22)	-0.040	25	—	-0.001(24)	0.005	25	—	0.009(26)	-0.003
30	0.037(46)	—	0.022	30	0.007(51)	—	0.034	30	0.013(55)	—	0.036
35	—	0.058(22)	0.036	35	—	0.007(22)	0.042	35	—	0.021(25)	0.054
40	0.026(48)	—	0.025	40	-0.088(51)	—	0.033	40	0.105(55)	—	0.039

$\mathcal{C}_{1,11,12}^{(3\nu)}(t)$			
$t$	H1-1	H1-1E	1-T
15	—	-0.047(24)	-0.034
20	0.062(56)	—	-0.020
25	—	-0.002(26)	0.025
30	-0.018(58)	—	0.069
35	—	0.062(27)	0.078
40	0.059(58)	—	0.062

TABLE S9. Results from Fig. S3 showing the three-body correlation  $\mathcal{C}_{1\nu N}^{(3\nu)}(t)$  for the  $N = 12$  neutrino system. The results computed using H1-1 were obtained using 240 shots, and those using H1-1E with 1200 shots. The column labeled “1-T” is the exact value using a single Trotter step.



$\mathcal{C}_{1,2,3}^{(3\nu)}(t)$				$\mathcal{C}_{2,3,4}^{(3\nu)}(t)$				$\mathcal{C}_{3,4,5}^{(3\nu)}(t)$			
$t$	H1-1	H1-1E	1-T	$t$	H1-1	H1-1E	1-T	$t$	H1-1	H1-1E	1-T
15	—	-0.017(20)	-0.011	15	—	0.017(17)	-0.004	15	—	-0.004(16)	-0.001
20	0.018(59)	—	-0.021	20	-0.033(57)	—	-0.008	20	-0.019(53)	—	-0.003
25	—	0.001(25)	-0.021	25	—	0.023(22)	-0.008	25	—	0.017(18)	-0.003
30	0.091(59)	—	-0.005	30	0.005(51)	—	-0.002	30	0.063(41)	—	-0.003
35	—	0.037(26)	0.004	35	—	-0.024(21)	0.007	35	—	-0.005(17)	-0.004
40	0.024(59)	—	-0.016	40	0.054(55)	—	0.012	40	0.101(39)	—	-0.014

$\mathcal{C}_{4,5,6}^{(3\nu)}(t)$				$\mathcal{C}_{5,6,7}^{(3\nu)}(t)$				$\mathcal{C}_{6,7,8}^{(3\nu)}(t)$			
$t$	H1-1	H1-1E	1-T	$t$	H1-1	H1-1E	1-T	$t$	H1-1	H1-1E	1-T
15	—	-0.025(17)	-0.0001	15	—	-0.011(15)	0.0001	15	—	-0.002(16)	-0.0001
20	-0.026(49)	—	-0.0001	20	-0.032(43)	—	0.0002	20	0.043(40)	—	-0.0002
25	—	0.008(16)	0.0005	25	—	0.003(14)	0.0003	25	—	0.002(14)	-0.0003
30	-0.017(31)	—	0.001	30	-0.022(16)	—	0.0003	30	-0.008(32)	—	-0.0003
35	—	-0.005(12)	-0.0001	35	—	-0.006(11)	-0.00003	35	—	-0.014(13)	0.00003
40	0.020(27)	—	-0.0005	40	-0.015(25)	—	-0.0002	40	0.019(13)	—	0.0002

$\mathcal{C}_{7,8,9}^{(3\nu)}(t)$				$\mathcal{C}_{8,9,10}^{(3\nu)}(t)$				$\mathcal{C}_{9,10,11}^{(3\nu)}(t)$			
$t$	H1-1	H1-1E	1-T	$t$	H1-1	H1-1E	1-T	$t$	H1-1	H1-1E	1-T
15	—	0.017(17)	0.0001	15	—	0.021(18)	0.001	15	—	-0.011(19)	0.004
20	0.044(43)	—	0.0001	20	0.013(37)	—	0.003	20	-0.013(45)	—	0.008
25	—	0.003(15)	-0.0005	25	—	0.004(19)	0.003	25	—	0.042(23)	0.008
30	0.001(32)	—	-0.001	30	0.011(40)	—	0.003	30	0.007(49)	—	0.002
35	—	0.002(11)	0.0001	35	—	0.007(16)	0.004	35	—	-0.012(20)	-0.007
40	-0.018(19)	—	0.0005	40	-0.013(35)	—	0.014	40	-0.025(48)	—	-0.012

$\mathcal{C}_{10,11,12}^{(3\nu)}(t)$			
$t$	H1-1	H1-1E	1-T
15	—	0.013(21)	0.011
20	0.055(53)	—	0.021
25	—	-0.021(25)	0.021
30	0.059(58)	—	0.005
35	—	0.026(26)	-0.004
40	0.001(58)	—	0.016

TABLE S10. Results from Fig. S3 showing the three-body correlation  $\mathcal{C}_{i-1,i,i+1}^{(3\nu)}(t)$  for the  $N = 12$  neutrino system. The results computed using H1-1 were obtained using 240 shots, and those using H1-1E with 1200 shots. The column labeled “1-T” is the exact value using a single Trotter step.

$\tau_4(t)$				$\tau_6(t)$		
$t$	H1-1	H1-1E	2-T	$t$	H1-1E	1-T
15	—	0.105(9)	0.115	17	0.008(2)	0.011
20	0.088(13)	—	0.073	27	0.002(1)	0.005
25	—	0.011(3)	0.001	37	0.058(7)	0.090
30	0.119(15)	—	0.148			
35	—	0.406(14)	0.484			
40	0.504(23)	—	0.629			

TABLE S11. Results from Fig. 4, showing the  $N$ -angle  $\tau_N$  for the  $N = 4$  and  $N = 6$  neutrino systems. The results computed using H1-1 were obtained using 480 shots, and those using H1-1E with 1200 shots. The column labeled “1-T” (“2-T”) is the exact value using a single (two) Trotter step.